J. Fluid Mech. (1991), *vol.* 225, *pp.* 271–300
Printed in Great Britain

Effect of a plane boundary on oscillatory flow around a circular cylinder

By B. M. SUMER, B. L. JENSEN AND J. FREDSØE
Technical University of Denmark, Institute of Hydrodynamics and Hydraulic Engineering, 2800 Lyngby, Denmark

(Received 19 January 1990 and in revised form 20 September 1990)

This study deals with the flow around a circular cylinder placed near a plane wall and exposed to an oscillatory flow. The study comprises instantaneous pressure distribution measurements around the cylinder at high Reynolds numbers (mostly at $Re \sim 10^5$) and a flow visualization study of vortex motions at relatively smaller Reynolds numbers ($Re \sim 10^3$–10^4). The range of the gap-to-diameter ratio is from 0 to 2 for the pressure measurements and from 0 to 25 for the flow visualization experiments. The range of the Keulegan–Carpenter number KC is from 4 to 65 for the pressure measurements and from 0 to 60 for the flow visualization tests. The details of vortex motions around the cylinder are identified for specific values of the gap-to-diameter ratio and for the KC regimes known from research on wall-free cylinders. The findings of the flow visualization study are used to interpret the variations in pressure with time around the pipe. The results indicate that the flow pattern and the pressure distribution change significantly because of the close proximity of the boundary where the symmetry in the formation of vortices breaks down, and also the characteristic transverse vortex street observed for wall-free cylinders for $7 < KC < 13$ disappears. The results further indicate that the vortex shedding persists for smaller and smaller values of the gap-to-diameter ratio, as KC is decreased. The Strouhal frequency increases with decreasing gap-to-diameter ratio. The increase in the Strouhal frequency with respect to its wall-free-cylinder value can be as much as 50% when the cylinder is placed very close to the wall with a gap-to-diameter ratio of $O(0.1)$.

1. Introduction

The effect of the close proximity of a wall on flow around a cylinder has been the subject of several investigations in recent decades. Various authors have developed theoretical models of potential flow around a cylinder, such as Milne-Thomson (1960) for a cylinder on a plane boundary, and Yamamoto, Nath & Slotta (1974) and Wright & Yamamoto (1979) for a cylinder close to a plane wall. Fredsøe & Hansen (1987) gave a modified description of the potential flow from which the lift force on the cylinder was evaluated.

Taneda (1964, 1965) reported qualitative and quantitative observations of the flow around a circular cylinder placed near a wall where the cylinder was towed in otherwise still fluid at constant velocity. Brown (1967), Bagnold (1974), Roshko, Steindfson & Chattoorgoon (1975) and Göktun (1975), on the other hand, were the first to measure lift and drag coefficients on cylinders on or near a wall in steady currents. Bearman & Zdravkovich (1978) measured the pressure distribution around a circular cylinder on and near a wall and also along the wall in steady currents. They

also conducted a spectral analysis of hot-wire signals received from both sides of the cylinder wake. From their spectral analysis, they found that regular vortex shedding persisted for values of gap-to-diameter ratio e/D down to about 0.3. This result was later confirmed by the measurements of Grass *et al.* (1984).

The case where the cylinder is subjected to an oscillatory flow has also attracted much attention, in view of its application to marine pipelines exposed to waves. The first investigation was that of Sarpkaya (1976*a*), followed by Sarpkaya (1977) and Sarpkaya & Rajabi (1979). Drag, inertia and lift coefficients on a cylinder placed at various distances from a wall were measured in these studies. Lundgren, Mathiesen & Gravesen (1976) measured the pressure distribution around a wall-mounted cylinder. Recently, Jacobsen, Bryndum & Fredsøe (1984), Ali & Narayanan (1986), Justesen *et al.* (1987) among others have reported measurements regarding the effect of the wall on force coefficients on a circular cylinder exposed to oscillatory flows.

Vortex flow regimes around a wall-free cylinder in oscillatory flows have been investigated in recent years by authors such as Bearman, Graham & Singh (1979), Singh (1979), Grass & Kemp (1979), Bearman & Graham (1979), Bearman *et al.* (1981) and most recently by Williamson (1985). These works have shed considerable light on the understanding of the complex behaviour of vortex motions in various regimes. Williamson, particularly, has been able to describe the vortex trajectory patterns in a systematic manner.

The present work is complementary to that by Bearman & Zdravkovich (1978) in the sense that it extends their study of flow around a near-wall cylinder in steady currents to the case of oscillatory flows, and is complementary to the work by Williamson (1985) in that it includes the effect of the close proximity of a wall on oscillatory flow around a circular cylinder. Here, the governing parameters are the Keulegan–Carpenter number, known from the wall-free cylinder research, the gap-to-diameter ratio which characterizes the effect of the wall proximity, plus of course the Reynolds number and the roughness parameter. This work basically focuses on the variations concerning the former two parameters.

The present study has practical relevance to the forces on and the hydroelastic vibrations of marine pipelines. Also, in the case of a loose sea bed, the vortex patterns around a marine pipeline have a large influence on the scour process in the vicinity of the pipe (Sumer & Fredsøe 1990).

2. Experimental set-up

2.1. *Pressure measurements*

The pressure measurements were made in a water flume 4 m wide, 1 m high and 28 m long. The circular cylinder used was an aluminium pipe of 9 cm in diameter and 2 m in length, the length-to-diameter ratio being about 22. The pipe was fixed to a vertical frame with two holders. The system comprising the cylinder and the frame was mounted on a carriage. The pipe could be placed at any distance from a wall. The wall was the bottom surface of a horizontal plate tapered at both ends. The plate itself was fixed to the carriage. See figure 1 for a schematic description of the test set-up.

The oscillating low was simulated by driving the carriage back and forth in otherwise still water. This was achieved by a hydraulic system where the movement of the carriage was controlled by a servo mechanism. With this arrangement, the carriage could be oscillated with a purely sinusoidal motion.

Twelve pressure transducers (Endevco Model 8510B-2 with a range of 0–2 p.s.i.

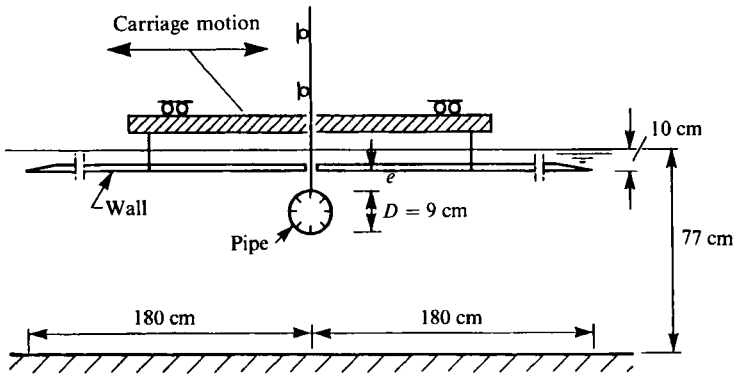

FIGURE 1. Sketch of the experimental system for pressure measurements.

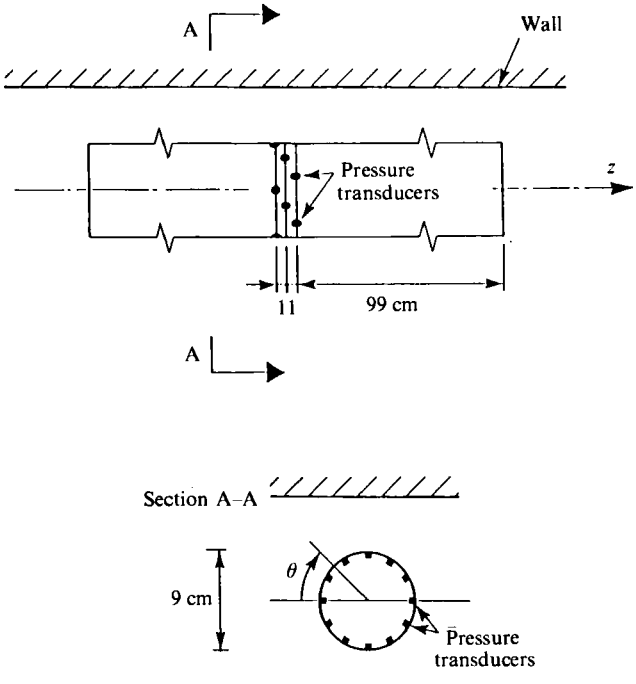

FIGURE 2. Layout of the pressure transducers.

and with a sensitivity of 150 ∓ 50 mV/p.s.i. at 10 V d.c. and 24 °C) were mounted on the surface of the cylinder at 30° intervals, the first one being at the angular location $\theta = 0°$ (see figure 2). Owing to the constructional constraints, the pressure transducers had to be mounted with a small offset in the z-direction, as indicated in figure 2.

To avoid complications which would arise otherwise owing to the close proximity of the wall there were no end plates. The fact that the measurement section was located sufficiently far away from the ends of the pipe (namely 11 diameters) justified such an arrangement.

Some supplementary tests were conducted with a rough-surface cylinder. The roughness was achieved by gluing a sheet of sandpaper on the cylinder surface. The roughness height of the sandpaper was measured to be $k = 0.35$ mm, and the density

Test series	Cylinder	Range of gap ratio e/D	Keulegan–Carpenter number $KC = U_m T/D$	Period T (s)	Cylinder Reynolds number $Re = U_m D/\nu$	Boundary-layer thickness to diameter ratio δ/D	Cylinder roughness parameter k/D
1	Smooth	0.05–2	4	0.83	0.4×10^6	0.01	—
			10	1.0	0.8×10^5	0.02	—
			20	1.67	1.0×10^5	0.03	—
			30	2.5	1.0×10^5	0.07	—
			55	4.2	1.1×10^5	0.14	—
			65	5.0	1.1×10^5	0.16	—
2	Rough	0–2	4	0.83	0.4×10^5	0.01	4×10^{-3}
			10	1.0	0.8×10^5	0.02	4×10^{-3}
			20	1.67	1.0×10^5	0.03	4×10^{-3}
			65	5.0	1.1×10^5	0.16	4×10^{-3}

TABLE 1. Test conditions for pressure measurements. The oscillatory boundary-layer thickness is calculated, using the information given in Jensen *et al.* (1989). In the rough-cylinder tests, the roughness elements were within the frequency boundary layer near separation, as δ_c/k is estimated to be in the range from about 2 to about 4. (δ_c is the cylinder boundary-layer thickness near separation.)

of protrusions was 80 grains/cm^2. This resulted in a Nikuradse's equivalent sand-roughness value of $k_s = 0.84$ mm.

Test conditions for the pressure measurements are summarized in table.1. In the table, the Keulegan–Carpenter number KC is defined by

$$KC = U_m T/D, \tag{1}$$

where D is the cylinder diameter, T the period of the oscillatory flow and U_m the maximum velocity defined by

$$U = U_m \sin(\omega t). \tag{2}$$

Here U is the flow velocity, t the time, and $\omega = 2\pi/T$ the angular frequency of the flow. The Reynolds number is defined by

$$Re = U_m D/\nu. \tag{3}$$

Other parameters in the table are e, the gap between the cylinder and the wall, and δ, the thickness of the oscillatory boundary layer which develops over the wall in the absence of the cylinder. Note that the boundary layer was transitional in all the tests except at $KC = 4$ (Jensen, Sumer & Fredsøe 1989).

Figure 3 gives sample pressure and force traces, where the forces are calculated by integrating the measured pressure distribution over the cylinder surface. Here, c_p is the pressure coefficient defined by

$$c_p = \frac{p - p_0}{\frac{1}{2}\rho U_m^2}, \tag{4}$$

where p is the pressure measured at the point under consideration and p_0 the hydrostatic pressure measured at the same point. F_x and F_y are respectively the in-line and the lift forces.

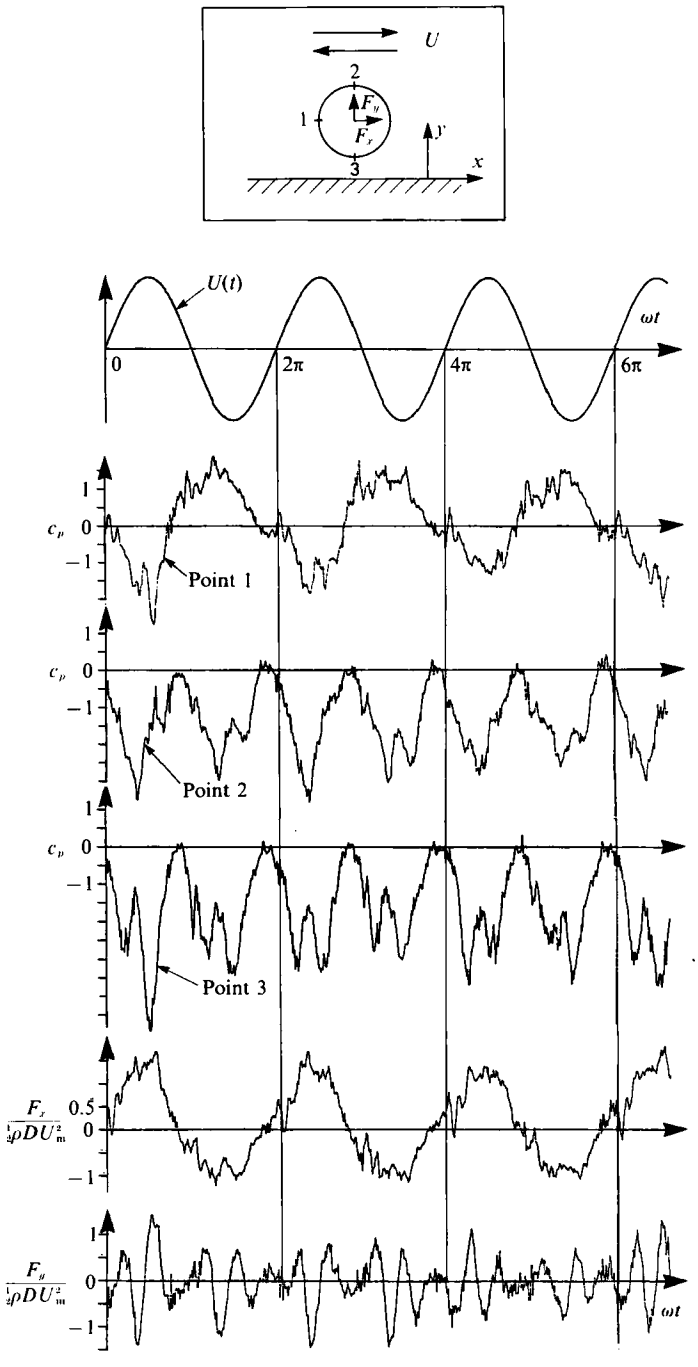

FIGURE 3. Sample pressure and force traces. $KC = 20$ and $e/D = 0.4$. Test series 1.

2.2. *Flow-visualization experiments*

The flow visualization experiments were conducted in a water tank with a working section 0.8 m high, 0.6 m wide and 3.0 m long. The experimental system comprised a circular cylinder (from 1 to 3 cm in diameter) and a flat plate tapered at both ends.

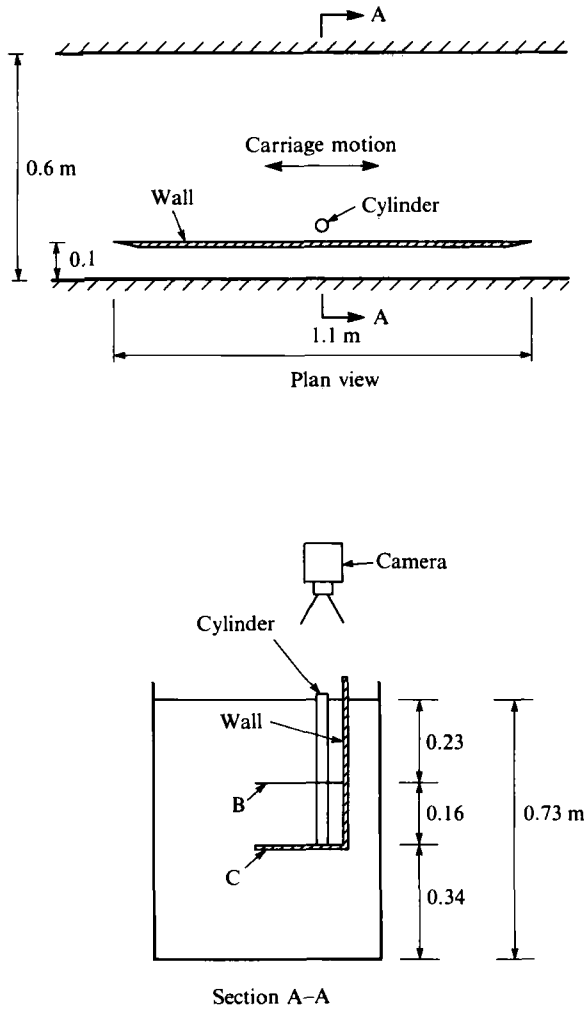

FIGURE 4. Sketch of the experimental system for flow visualization. B: plate of size $40 \times 25 \times 0.1$ cm. C: bar of size $25 \times 1.5 \times 1.5$ cm holding the cylinder.

This system was mounted vertically onto a carriage. The cylinder could be placed at any desired position with respect to the plate. Again, the oscillatory flow was created by oscillating the carriage with a sinusoidal motion. Aluminium powder sprinkled onto the water surface was used as flow tracer in the experiments.

The flow processes around the cylinder were video taped. Figure 4 gives a schematic description of the test set-up. The range of KC was from about 0 up to 60, the upper portion of the range, from 35 to 60, being achieved with a cylinder diameter $D = 1$ cm. The range of the gap-to-diameter ratio e/D was from 0 to 25 for $D = 1$ cm and from 0 to 8 for $D = 3$ cm. The ratio of the boundary-layer thickness to the diameter was $\delta/D = 0.04$ and 0.19, corresponding to $KC = 4$ and 60, respectively. The Re-range of the experiments was 10^3–10^4. Thus the results of the present flow visualization study are applicable only to subcritical flow regimes. However, it might be expected that the picture regarding the various vortex flow regimes would remain the same for the other KC regimes.

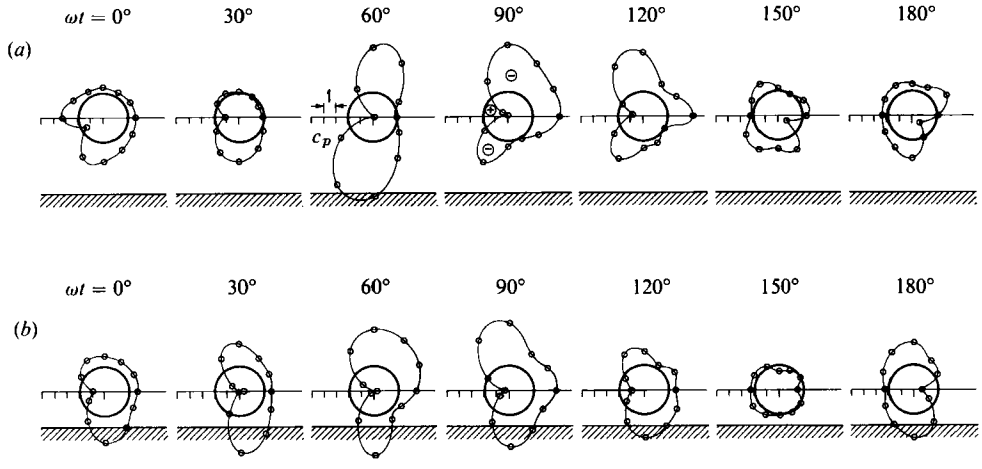

FIGURE 5. Evolution of instantaneous pressure distribution during one half-cycle of motion. $KC = 10$. Test series 1. (*a*) $e/D = 1$, (*b*) $e/D = 0.2$.

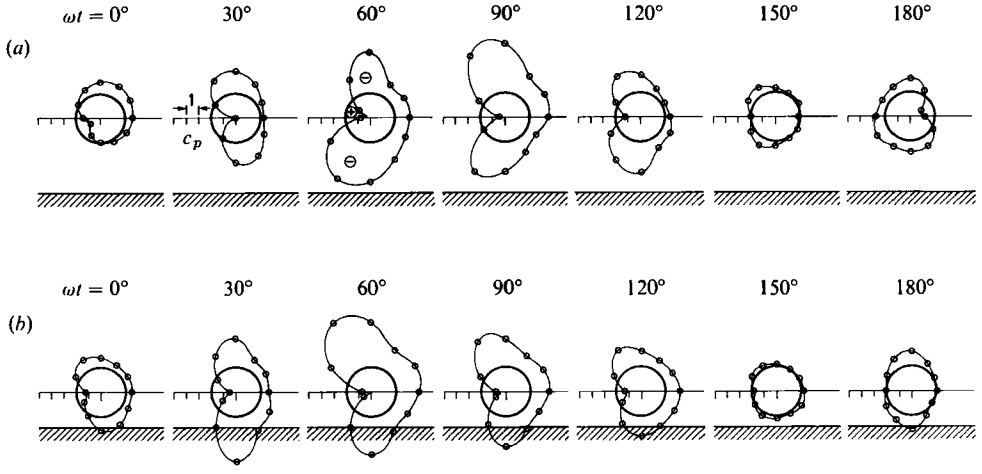

FIGURE 6. Evolution of instantaneous pressure distribution during one half-cycle of motion. $KC = 20$. Test series 1. (*a*) $e/D = 1$, (*b*) $e/D = 0.2$.

3. Experimental results and discussion

3.1. *Pressure distributions*

Figures 5 and 6 illustrate the time evolution of instantaneous pressure distributions during one half-period of the motion for two values of KC, namely 10 and 20. The pressure distribution patterns have been found to be quite repeatable from one period to another, although they may experience some occasional changes.

From figures 5 and 6 the following observations can be made. First, the stagnation point, which is characterized by the maximum, positive value of c_p, moves to the lee side of the cylinder before the free-stream flow reverses. Secondly, the distribution patterns change sharply at some phase values during the course of the motion (See, for example, the change in the pressure distribution in figure 5(*a*) in the phase interval from $\omega t = 60°$ to 90°; and in figure 5(*b*) from $\omega t = 60°$ to 90°, and also similar changes in figure 6). These changes are associated with the vortex shedding

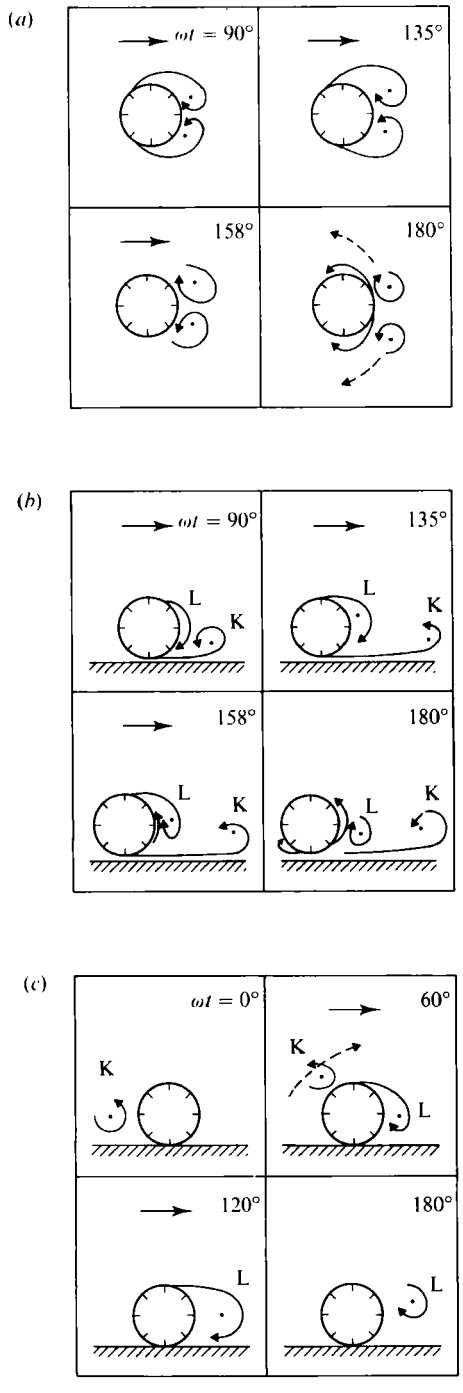

FIGURE 7. Evolution of vortex motions. $KC = 4$. Test series 1. (*a*) $e/D = 2$, (*b*) $e/D = 0.1$, (*c*) $e/D = 0$.

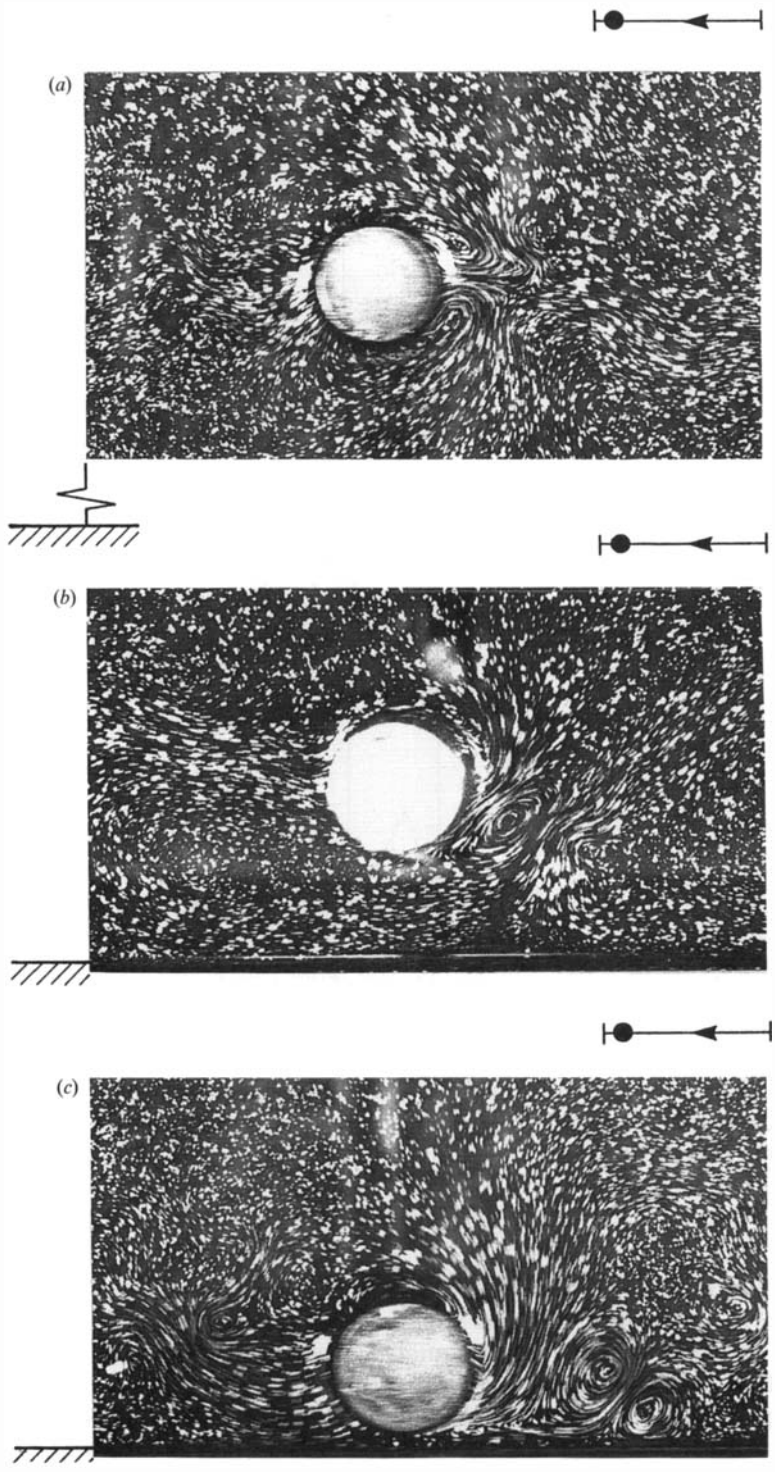

FIGURE 8. Photographs showing the establishment of asymmetry due to the close proximity of the wall. $KC = 4$. (*a*) $e/D = 3.5$, (*b*) $e/D = 1$, (*c*) $e/D = 0.1$.

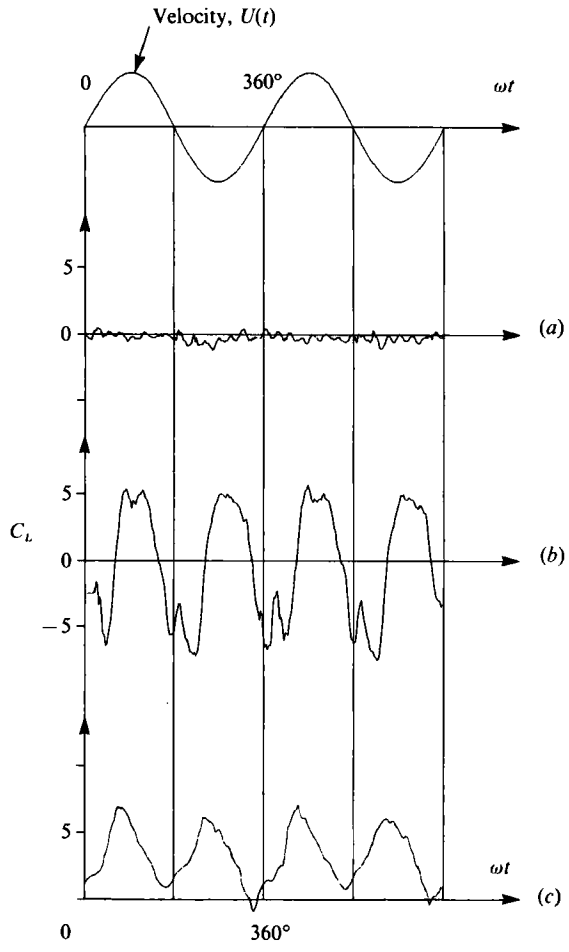

FIGURE 9. Lift-force traces. $KC = 4$. (*a*) and (*b*) Test series 1 for $e/D = 2$ and 0.1 respectively. (*c*) Test series 2 for $e/D = 0$.

phenomenon, as will be explained later. Thirdly, placing the cylinder nearer the wall generally increases the pressure (i.e. decreases the negative pressure) on the wall-side surface of the cylinder.

3.2. *Vortex flow regimes*

3.2.1. $4 < KC < 7$

Figure 7 illustrates how the vortices evolve during the course of the oscillatory motion for $KC = 4$. The flow sketches in this and in the following figures were traced directly from the video screen. The symmetry observed in the formation and also in the motion of the vortices (figure 7*a*) disappears when $e/D = 0.1$ (figure 7*b*); see also the photograph in figure 8. This is also clear from the lift-force traces given in figure 9, where almost no lift force is exerted on the cylinder for $e/D = 2$, while a non-zero lift exists for $e/D = 0.1$. Here C_L is the lift coefficient defined by

$$F_y = \tfrac{1}{2}\rho C_L D U_m^2. \tag{5}$$

For a wall-free cylinder the symmetry breaks up when the KC exceeds 4–5

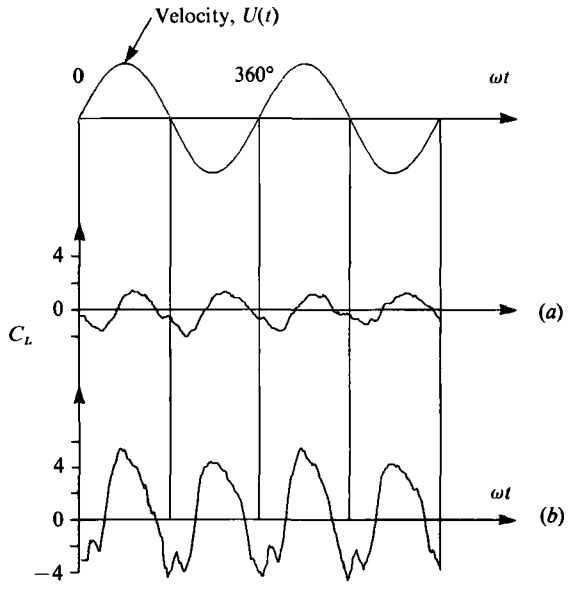

FIGURE 10. Lift-force traces. $KC = 6$. Test series 1: (*a*) $e/D = 2$, (*b*) $e/D = 0.1$.

(Williamson 1985), so a non-zero lift will also be present for this latter case (figure 10*a*).

The vortex regime is quite simple for the wall-mounted cylinder (figure 7*c*): a vortex grows behind the cylinder each half-period, and is washed over the cylinder as the next half-period progresses. The lift-force trace is presented in figure 9. The peaks in the lift force are associated with the occurrences where the vortices (Vortex K, Vortex L, ... in figure 7*c*) are washed over the cylinder.

3.2.2. $7 < KC < 15$

One of the interesting features of this KC range for a wall-free cylinder is the formation of the so-called transverse vortex street where the shed vortices form a vortex street perpendicular to the flow direction, as demonstrated by Bearman (1985), Williamson (1985) and Sarpkaya (1987). Williamson (1985) reports that the transverse vortex street regime exists for quite a wide range of KC in this interval, namely for $7 < KC < 13$, while for the rest of the interval ($13 < KC < 15$), the transverse street regime degenerates into the so-called 'single pairs' regime. (In this latter regime, the wake consists of a series of vortex pairs convecting away each period at around 45° to the flow oscillation direction and on one side of the cylinder only.)

The visualization tests conducted in the present study, with a cylinder placed at different positions from a wall, have shown that the transverse street regime disappears when the gap between the cylinder and the wall becomes less than about 1.7. Figure 11(*a*) and 11(*b*) illustrate two different vortex flow regimes, one with a gap ratio above this critical value (the transverse street regime) and the other below it, where the transverse vortex street is replaced by a wake region which lies parallel to the flow oscillation direction.

(*a*) $e/D = 1$. Figure 12(*a*) illustrates the time development of vortex motions during one half-period of the motion, while figure 13(*b*) presents the corresponding lift-force trace. Figure 12(*a*) indicates that there is only one vortex shed (Vortex L)

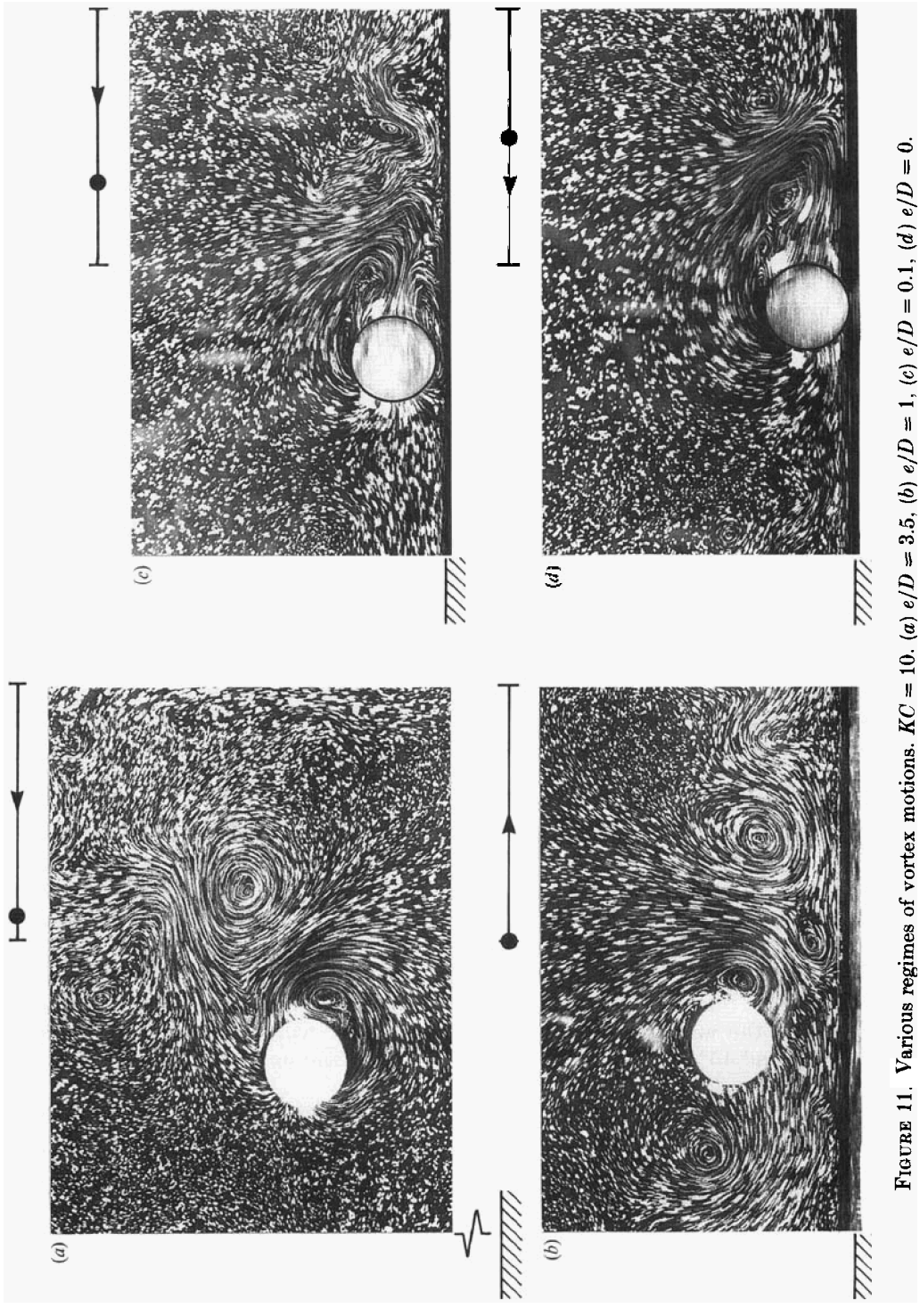

FIGURE 11. Various regimes of vortex motions. $KC = 10$. (*a*) $e/D = 3.5$, (*b*) $e/D = 1$, (*c*) $e/D = 0.1$, (*d*) $e/D = 0$.

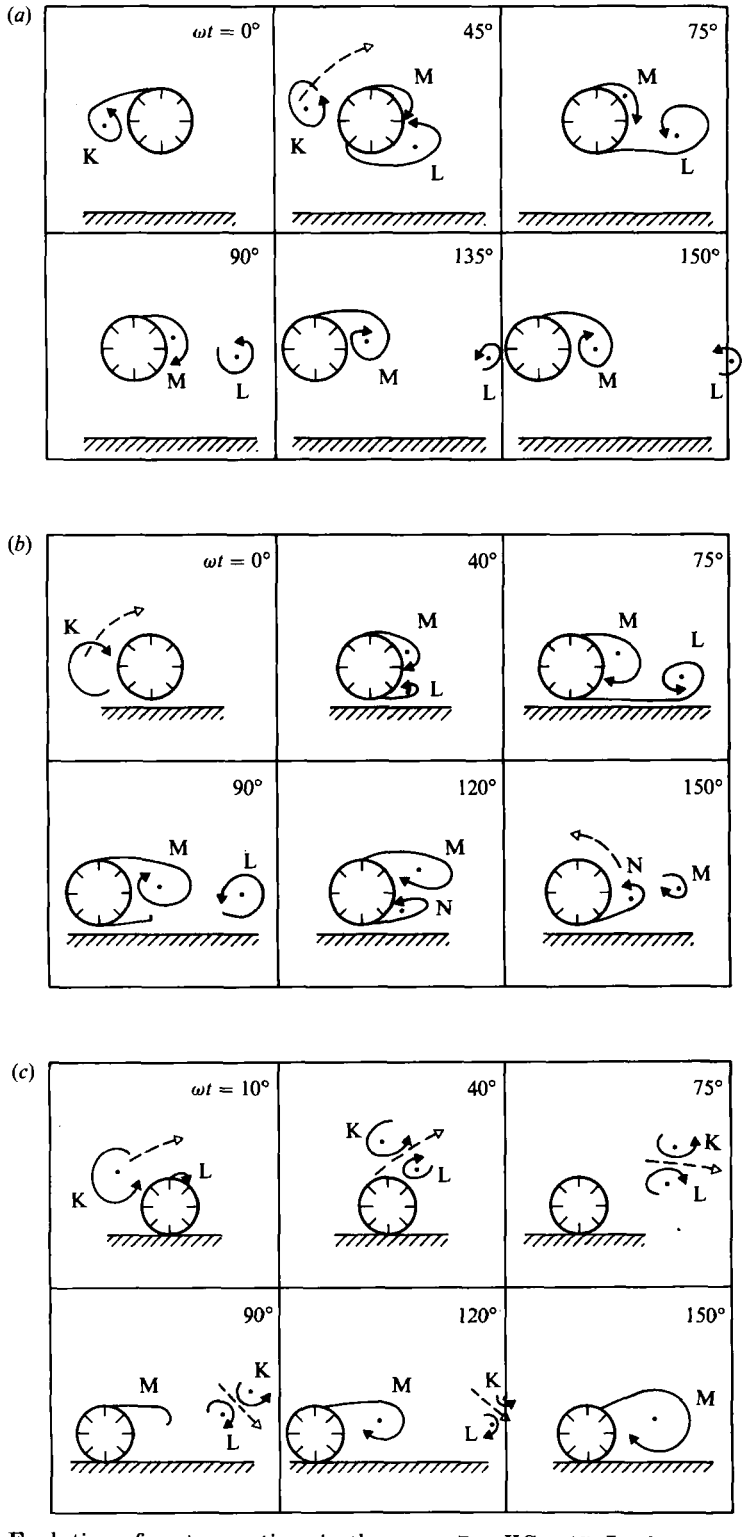

FIGURE 12. Evolution of vortex motions in the range $7 < KC < 15$. In the tests presented here $KC = 10$. (*a*) $e/D = 1$, (*b*) $e/D = 0.1$, (*c*) $e/D = 0$.

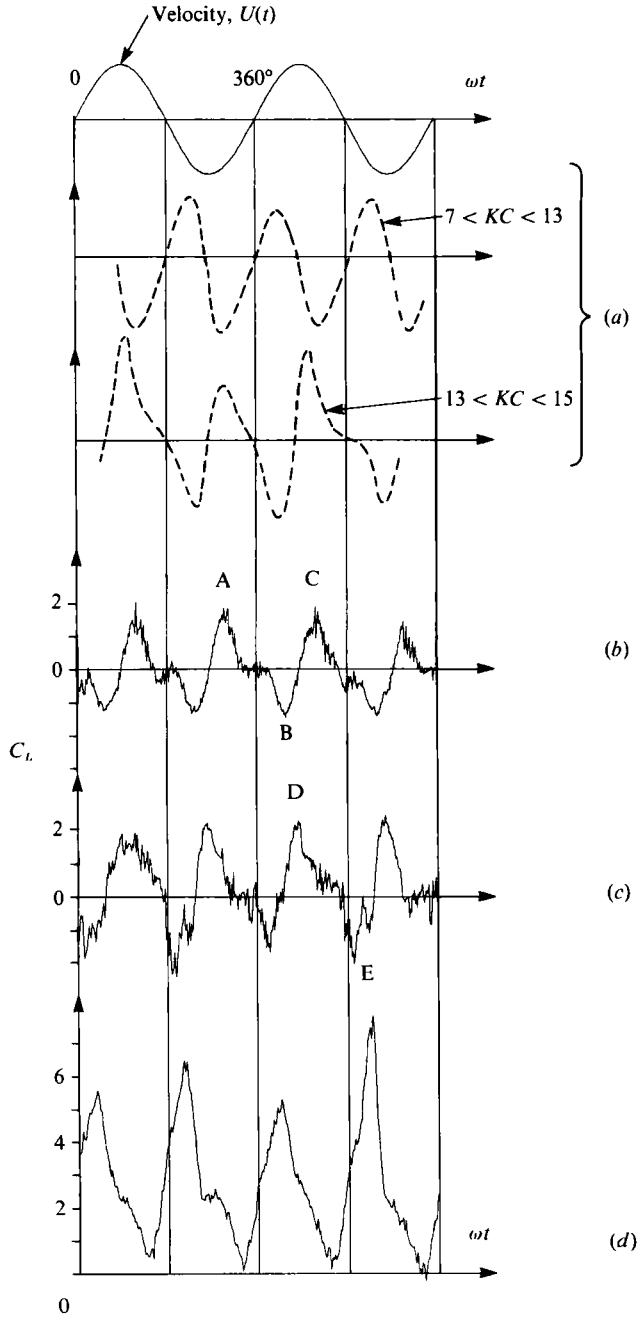

FIGURE 13. Lift-force traces in the range $7 < KC < 15$. Positive lift is directed away from the wall. The wall-free cylinder traces (*a*), $e/D = \infty$, are taken from Williamson (1985). (*b*) and (*c*) Test series 1 at $e/D = 1$ and 0.1 respectively; and (*d*) Test series 2 at $e/D = 0$. For the tests presented here $KC = 10$.

during one half-period of the motion. Figure 13(*b*) shows how the lift force evolves during the course of the motion. The negative peak (B in figure 13*b*) is caused by Vortex *K* (figure 12*a*, $\omega t = 0°$–$45°$) (see Maull & Milliner 1978 for the relation between the vortex motion and the forces). As Vortex *K* is washed over the cylinder, the

cylinder experiences a positive lift force, and the development of Vortex L also exerts a positive lift force (C in figure 13*b*). As Vortex L moves away from the cylinder ($\omega t = 135°$–$150°$), the positive lift exerted on the cylinder by Vortex L is diminished.

It is apparent that the manner in which the lift force varies with time in the present case (figure 13*b*) is different from that when $e/D = \infty$ and $7 < KC < 13$ (figure 13*a*). This is because the vortex motions in the two situations are entirely different.

(*b*) $e/D = 0.1$. The main difference between this case and the previous one is that here the wall-side vortex (Vortex N) grows quite substantially. It is this latter vortex which is washed over the cylinder, whereas in the former case it was the free-stream-side vortex (Vortex M).

The positive peak in the lift force (D in figure 13*c*) is caused by the development of Vortex L. The negative peak in the lift force (E in figure 13*c*), on the other hand, is caused by the motion of Vortex N across the cylinder, combined with the high velocities in the gap induced by the flow reversal.

(*c*) $e/D = 0$. In this case, the vortex which develops behind the cylinder in the previous half-period (Vortex K in figure 2*c*) and the vortex which is newly created (Vortex L in figure 12*c*) form a vortex pair. This pair is then set into motion owing to its self-induced velocity field, and thus steadily moves away from the cylinder in the downstream direction (see figure 12*c*), $\omega t = 40°$–$120°$). Following the removal of Vortex L, a new vortex (Vortex M) begins to develop behind the cylinder.

The visualization results show that the way in which the vortex flow regime develops for the wall-mounted cylinder ($e/D = 0$) remains the same, irrespective of the range of KC. It should be noted, however, that the individual events such as the formation of the vortex pair etc. may occur at different phase (ωt) values for different KC ranges.

The peaks in the lift-force trace are caused by the passage of Vortex K over the cylinder.

3.2.3. $15 < KC < 24$

(*a*) $e/D = 1$. In this KC regime there is no symmetry between the half-periods, as far as the vortex motions are concerned (Williamson 1985), and this also applies to the present case where $e/D = 1$, as seen from figure 14(*a*); the vortex which is washed over the cylinder alternates between the wall side and the free-stream side each half-period. The lift-force variation (figure 15*b*) supports this asymmetric flow picture. The variations in the lift force can be interpreted in terms of the vortex motions, as described above.

(*b*) $e/D = 0.1$. Here, the asymmetry in the vortex motion from one half-period to the next observed in the previous case disappears; it is always the wall-side vortex (Vortex P, figure 14*b*) which is washed over the cylinder before the flow reverses to start a new half-period.

The lift force is directed away from the wall most of the time (figure 15*c*). Furthermore, it contains distinct, short-duration peaks in its variation with time (F, G in figure 15*c*). The flow-visualization tests show that these peaks are associated with the vortex shedding at the wall side of the cylinder: such peaks occur whenever there is a growing vortex on that side of the cylinder (figure 14*b*: $\omega t = 50°$–$60°$ and $\omega t = 80°$–$93°$).

Figure 16 represents the lift-force traces separately for the interval $0.05 \leqslant e/D \leqslant 0.4$. For values of the gap ratio smaller than approximately 0.3, the lift force becomes asymmetric, being directed away from the wall for most of the time, containing the

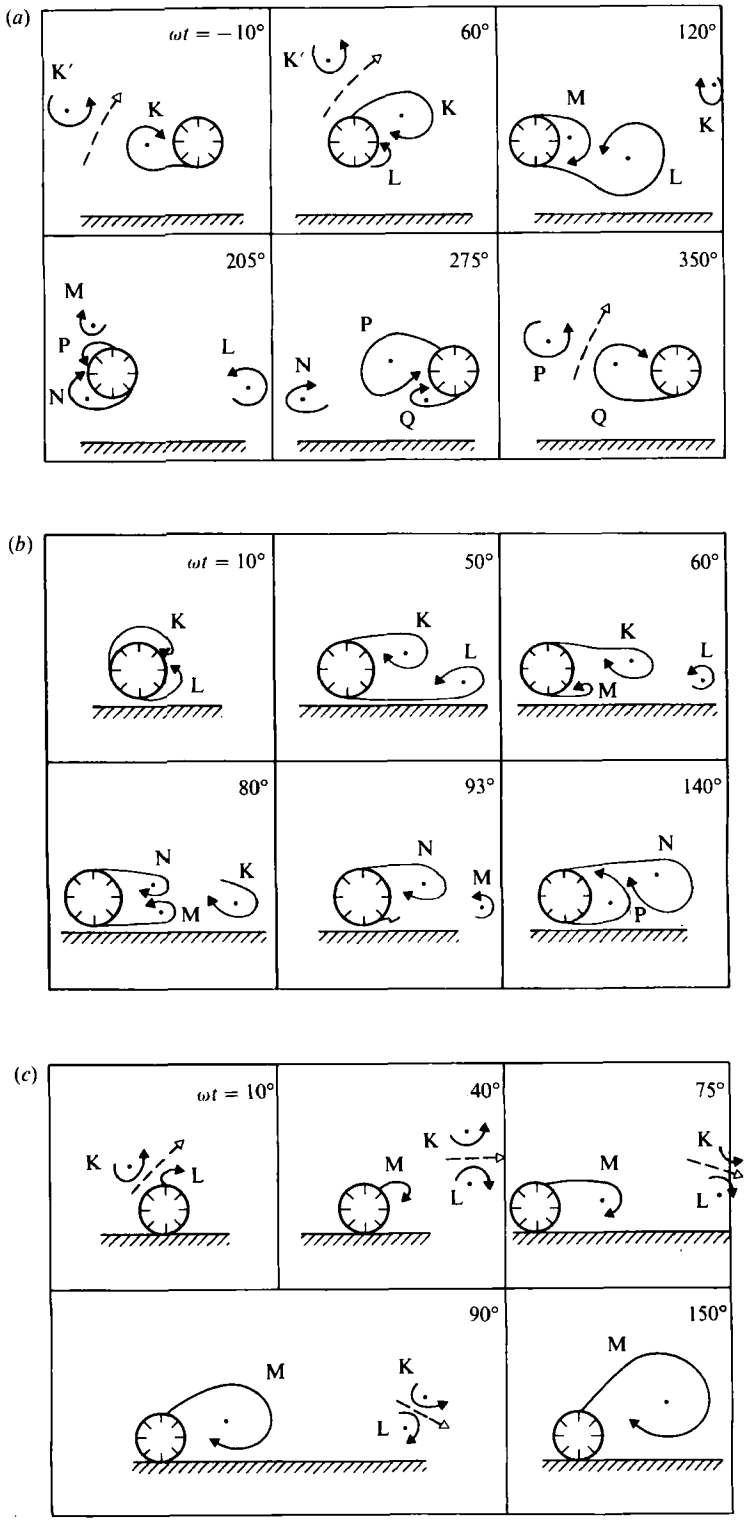

FIGURE 14. Evolution of vortex motions in the range $15 < KC < 24$. In the tests presented here $KC = 20$. (*a*) $e/D = 1$, (*b*) $e/D = 0.1$, (*c*) $e/D = 0$.

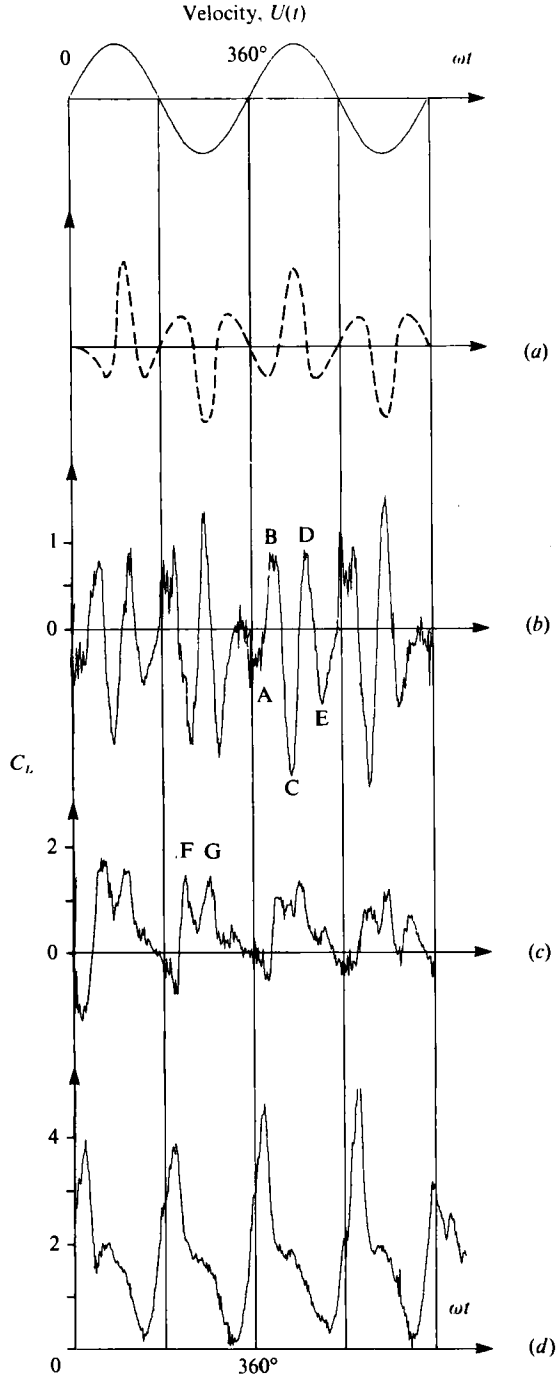

FIGURE 15. Lift-force traces in the range $15 < KC < 24$. Positive lift is directed away from the wall. The wall-free cylinder ($e/D = \infty$) trace (*a*) is taken from Williamson (1985). (*b*) and (*c*) Test series 1 with $e/D = 1$ and 0.1 respectively; and (*d*) Test series 2 with $e/D = 0$. In the tests presented here $KC = 20$.

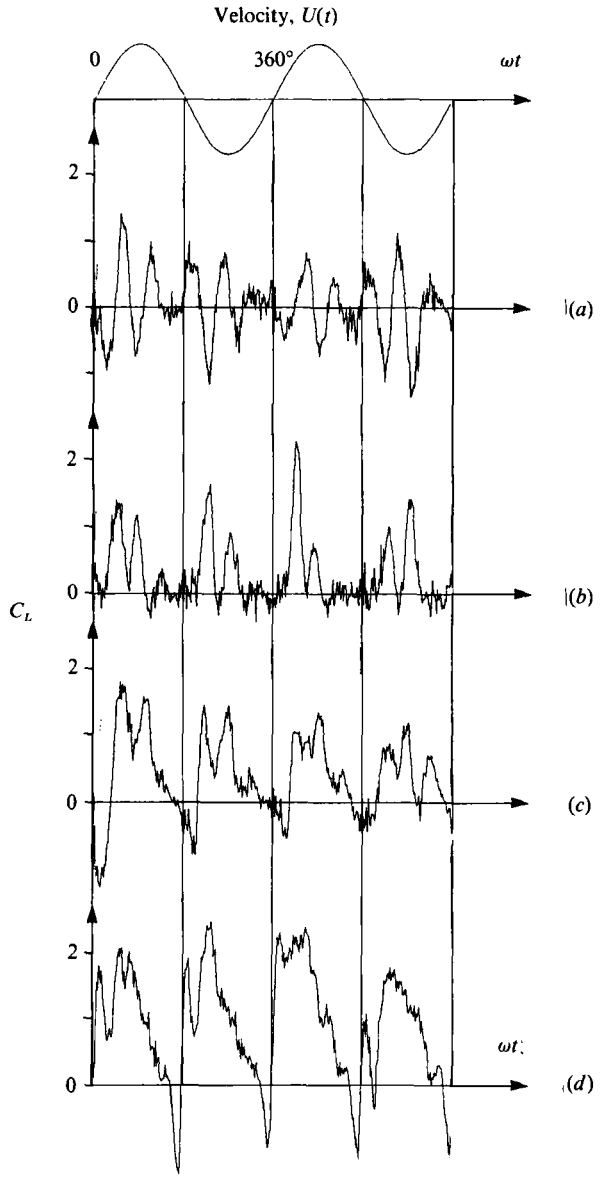

FIGURE 16. Lift-force traces for the ranges $0.05 \leqslant e/D \leqslant 0.4$ and $15 < KC < 24$. Positive lift is directed away from the wall. Test series 1. In the tests presented here $KC = 20$. (*a*) $e/D = 0.4$, (*b*) $e/D = 0.2$, (*c*) $e/D = 0.1$, (*d*) $e/D = 0.05$.

previously mentioned distinct, short-duration peaks. These peaks are present even for the gap ratio $e/D = 0.05$. These short-duration peaks imply that the vortex shedding is maintained even for very small gap ratios such as $e/D = 0.1$, in contrast to what occurs in steady currents where the vortex shedding is maintained for values of gap ratio down to only about $e/D = 0.3$, as demonstrated by Bearman & Zdravkovich (1978). This aspect of the problem will be discussed in greater detail in §3.3.1.

(*c*) $e/D = 0$. It is apparent from figure 14(*c*) that the manner in which the vortex flow regime develops is exactly the same as in the range $7 < KC < 15$ (cf. figures 12*c*

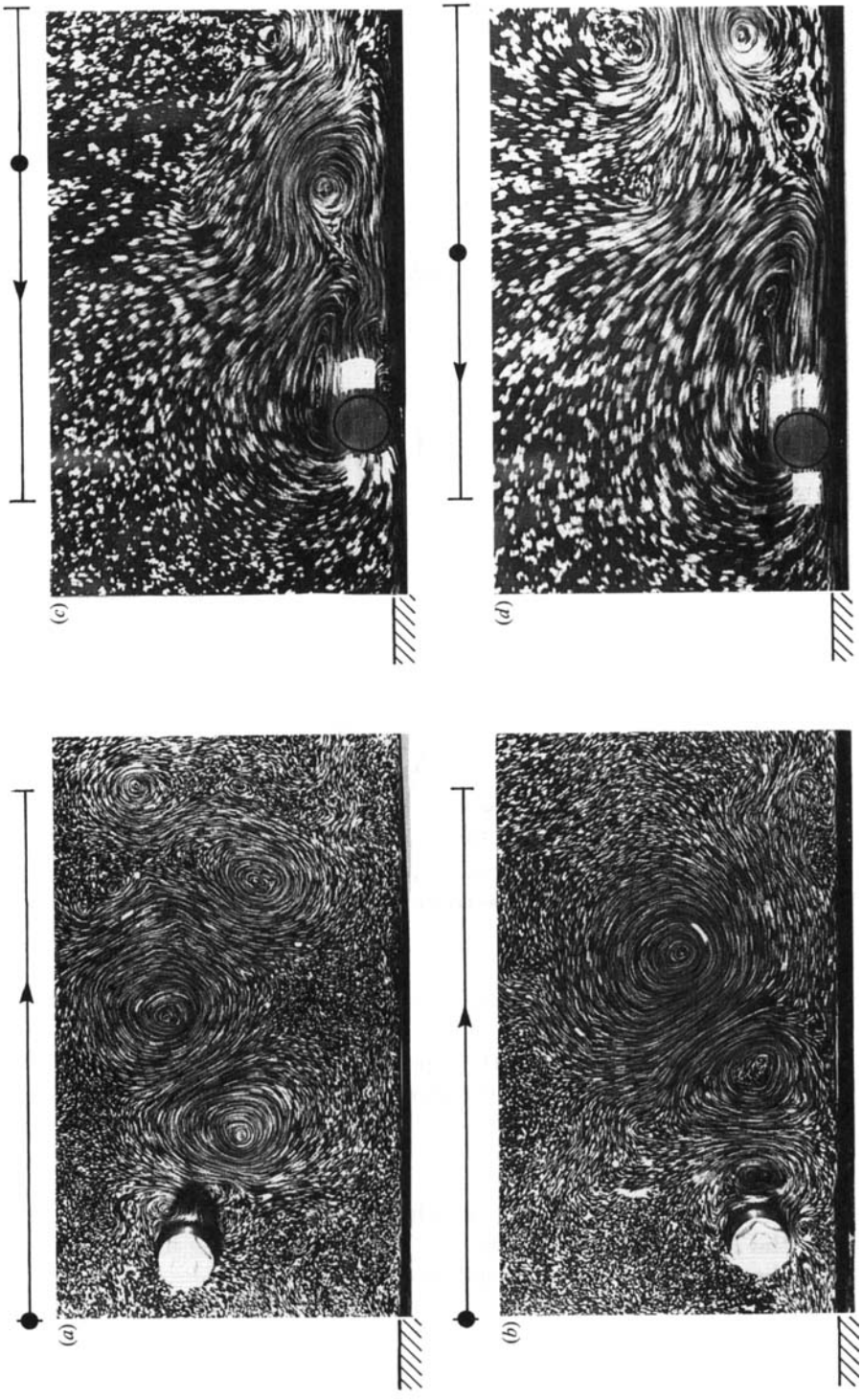

FIGURE 17. Regimes of vortex motions. $KC = 30$. (*a*) $e/D = 3.5$, (*b*) $e/D = 1$, (*c*) $e/D = 0.1$ and (*d*) $e/D = 0$.

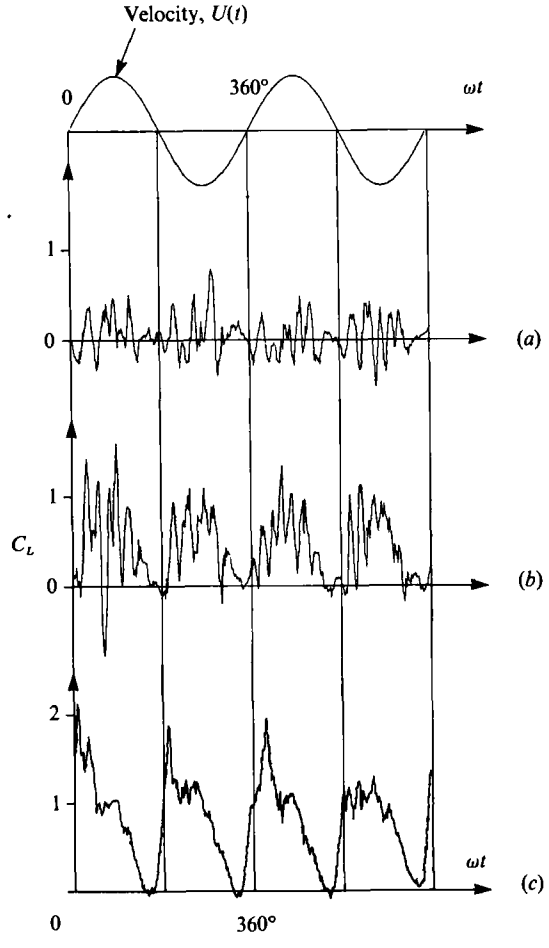

FIGURE 18. Lift-force traces in the range $KC > 24$. Positive lift is directed away from the wall. (*a*) and (*b*) Test series 1 at $e/D = 1$ and 0.1 respectively; and (*c*) Test series 2 at $e/D = 0$. In the tests presented here $KC = 65$.

and 14*c*). However, the streamwise distance that the vortex pair travels is now relatively larger.

The lift force (figure 15*d*) varies with respect to time in the same way as in figure 13(*d*) where $7 < KC < 15$. However, the peaks in the present case occur relatively earlier than those in figure 13(*d*).

3.2.4. $KC > 24$. *Further KC regimes*

The present visualization tests indicate that, like in Williamson (1985), the flow patterns for the KC regimes beyond $KC = 24$ differ only in the number of vortices shed with no basic changes in the actual flow patterns.

Figure 17 presents visualization photographs, illustrating the flow patterns corresponding to four different gap-to-diameter ratios, including the wall-mounted cylinder case. Figure 18 presents sample lift-force traces for three different values of e/D, namely 1, 0.1 and 0. Similar comments to those made in §3.2.3 apply to this case, too.

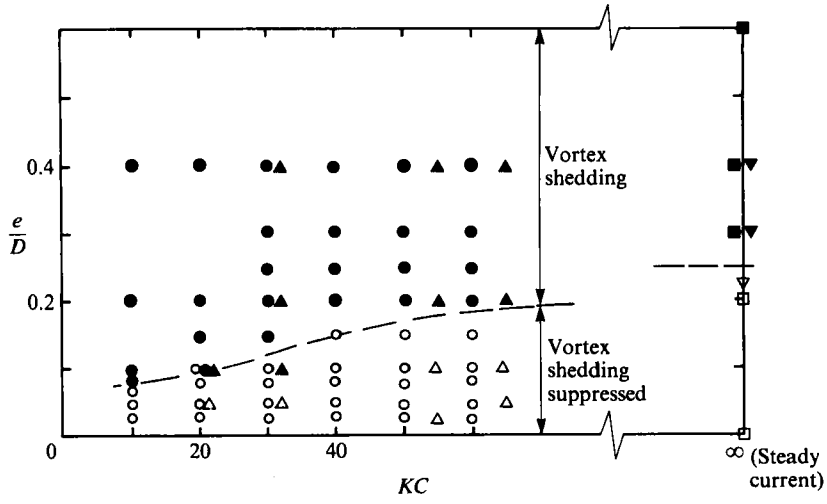

FIGURE 19. Diagram showing where the vortex shedding is suppressed in the (e/D, KC)-plane. Open symbols: vortex shedding is suppressed. Filled symbols: vortex shedding exists. ○, △, Present experiments (○ from flow visualization, △ from lift-force traces); □, Bearman & Zdravkovich (1978); ▽, Grass *et al.* (1984).

3.3. *Vortex shedding*

3.3.1. *Suppression of vortex shedding*

Whether vortex shedding will be suppressed for small values of the gap ratio can be detected from the flow-visualization films as well as from the lift-force traces. The results of such an analysis in the present study are plotted in figure 19. From the figure, the following observations can be made.

(*a*) For large values of KC, it appears that the gap ratio below which the vortex shedding is suppressed approaches the critical value $e/D \approx 0.25$ deduced from the work by Bearman & Zdravkovich (1978) and by Grass *et al.* (1984) for steady currents.

(*b*) Although the borderline between the two regions in the figure, namely the vortex-shedding region and the region where the vortex shedding is suppressed, is not expected to be a clean-cut curve, there is a clear tendency that the vortex shedding is maintained for smaller and smaller values of the gap ratio as KC is decreased.

Vortex shedding is maintained even for very small gap ratios such as $e/D = 0.1$ for $KC = 10$–20, as shown in the photograph in figure 11 (*c*). Likewise, figure 16 (*c*) implies that shedding occurs for that value of the gap ratio, as the short-duration peaks in the lift-force time series are associated with vortex shedding. The reason why vortex shedding is maintained for such small gap ratios may be because the water discharge at the wall side of the cylinder is much larger in oscillatory flow at small KC than in steady currents.

3.3.2. *Strouhal-number variation*

Figure 20 presents the Strouhal number, St, plotted against the gap ratio for various values of KC. Here, St is defined by

$$St = fD/U_{\mathrm{m}}, \tag{6}$$

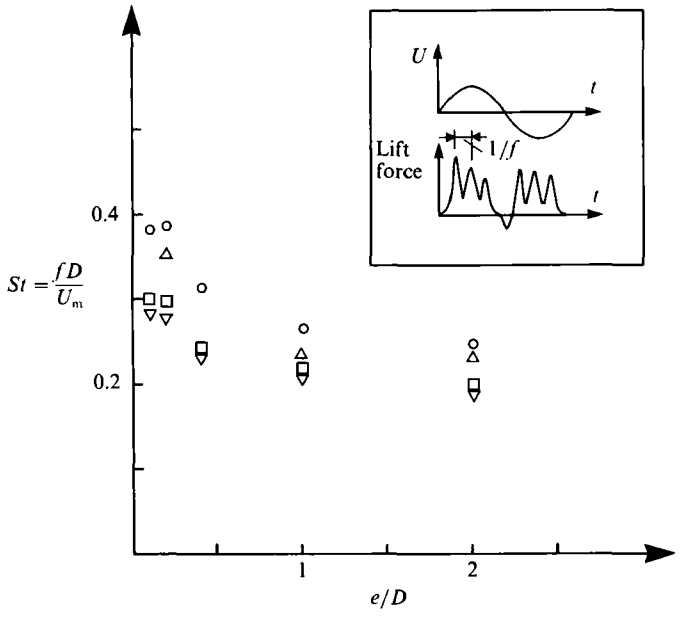

FIGURE 20. Strouhal number versus gap ratio. Test series 1. ○, $KC = 20$; △, $KC = 30$; □, $KC = 55$; ▽, $KC = 65$.

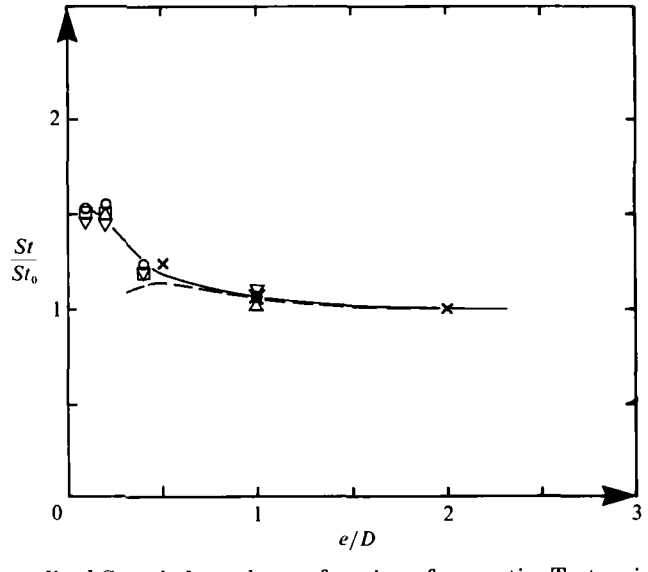

FIGURE 21. Normalized Strouhal number as function of gap ratio. Test series 1. ○, $KC = 20$; △, $KC = 30$; □, $KC = 55$; ▽, $KC = 65$; ×, steady current (Raven *et al.* (1985); ---, steady current (Grass *et al.* 1984).

where f is the vortex shedding frequency obtained from the lift-force data. As seen for example from figure 18(*a*, *b*), the shedding frequency actually varies over the cycle. The f-value used in the definition of St in the preceding equation is averaged over a sufficiently long period of time. Figure 21 presents the same data in the normalized form St/St_0 where St_0 is the value of St attained for large values of e/D.

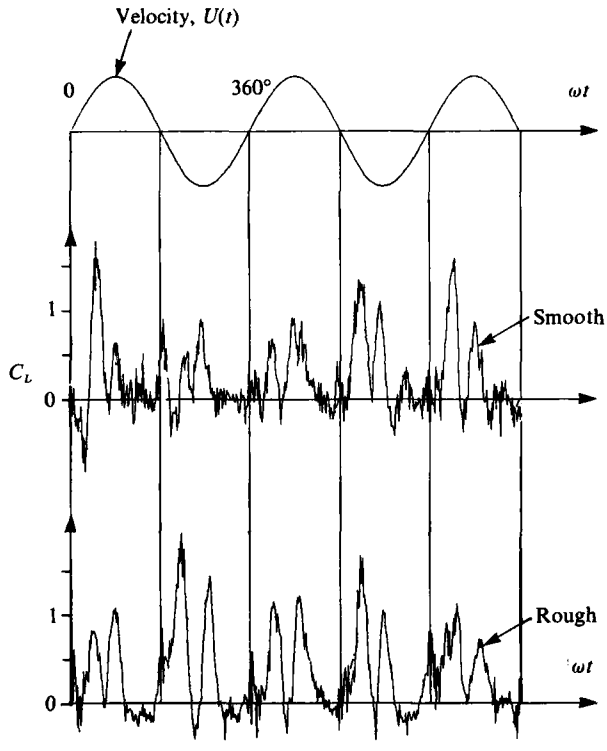

FIGURE 22. Lift-force traces for smooth (Test series 1) and rough cylinders (Test series 2). $KC = 20$. $e/D = 0.2$.

Also plotted in figure 21 are the results of two studies conducted in steady currents, namely Grass *et al.* (1984) and Raven, Stuart & Littlejohns (1985). Grass *et al.*'s experiments were done in a laboratory channel with both smooth and rough beds. The surface of the test cylinder was smooth. Their results collapse onto a common curve when plotted in the normalized form presented in figure 21. The data points of Raven *et al.*'s study, on the other hand, were obtained in an experimental program conducted in the Severn Estuary (UK) where a full-scale pipeline (50.8 cm in diameter with a surface roughness of $k/D = 8.5 \times 10^{-3}$) was used. In both studies, St is defined by the velocity at the top of the cylinder.

From figures 20 and 21 the following conclusions can be drawn.

(*a*) For a given e/D, St increases (albeit slightly) with decreasing KC (figure 20).

(*b*) The measurements collapse remarkably well when plotted in the normalized form St/St_0 versus e/D (figure 21), where the influence of the close proximity of the wall on St can be seen even more clearly.

(*c*) It is apparent that St increases as the gap ratio decreases. The increase in St frequency can be considerable (by as much as 50%) when the cylinder is placed very near the wall ($e/D = 0.1$–0.2), because the presence of the wall causes the wall-side vortex to be formed closer to the free-stream-side vortex. As a result of this, the two vortices interact at a faster rate, leading to a higher St frequency.

3.3.3. *Influence of cylinder roughness*

Figure 22 presents lift-force traces obtained for both the smooth- and rough-surface cylinders for $KC = 20$, the gap ratio e/D being 0.2. It is apparent that the

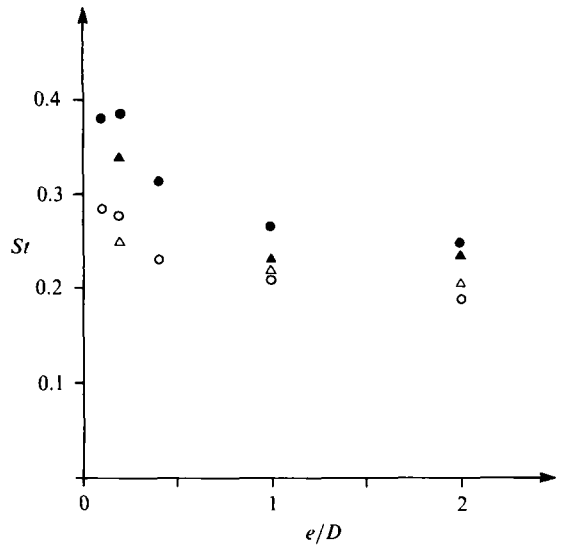

FIGURE 23. Strouhal number versus gap ratio. ○, Smooth cylinder (Test series 1); △, rough cylinder (Test series 2). Filled symbols, $KC = 20$; open symbols, $KC = 65$.

manner in which the lift force varies with respect to time remains unchanged, irrespective of whether the cylinder has a smooth or a rough surface. Similar observations have been made for the other KC values.

Figure 23 compares the smooth-cylinder St data with the rough cylinder ones. Again, there is almost no noticeable difference between the results.

3.4. *Force coefficients*

3.4.1. *Smooth cylinder*

Figures 24 and 25 present the force-coefficient data obtained from the present pressure measurements. Here, the force coefficients are defined by

$$F_x = \tfrac{1}{2}\rho C_d D U(t)\,|U(t)| + \tfrac{1}{4}\pi\rho D^2 C_a \frac{\mathrm{d}U}{\mathrm{d}t}, \tag{7}$$

$$F_{y\mathrm{A}} = \tfrac{1}{2}\rho C_{L\mathrm{A}} D U_{\mathrm{m}}^2, \tag{8}$$

$$F_{y\mathrm{T}} = \tfrac{1}{2}\rho C_{L\mathrm{T}} D U_{\mathrm{m}}^2, \tag{9}$$

where C_d is the drag coefficient, C_a the added-mass coefficient, $F_{y\mathrm{A}}$ the maximum value of the lift force away from the wall and $F_{y\mathrm{T}}$ that towards the wall. The coefficient C_a is related to the inertia coefficient C_M through

$$C_M = C_a + 1. \tag{10}$$

Also included in the figures are Sarpkaya's (1977) and Sarpkaya & Rajabi's (1979) results for smooth cylinders at $Re = 10^5$. It appears that the present data are generally in accord with these.

From the figures, the data indicate that the force coefficients C_d, C_M and $C_{L\mathrm{A}}$ increase as the gap ratio decreases. This is also true for $C_{L\mathrm{T}}$ for small KC ($O(10)$). For large KC, however, no clear trend appears.

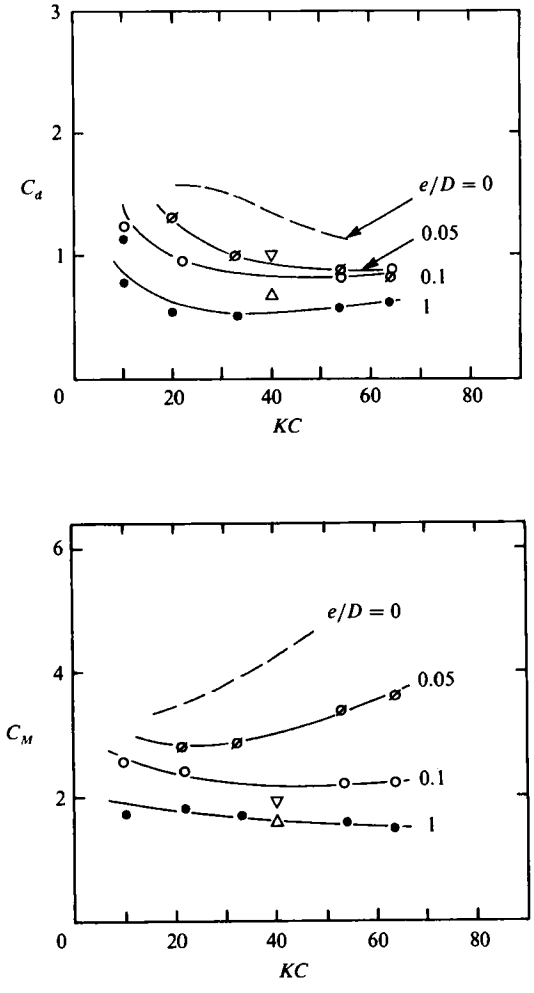

FIGURE 24. Drag and inertia coefficients. Smooth cylinder (Test series 1). ○, Present data ($Re = 0.8 \times 10^5$–1.1×10^5); △, $e/D = 1$; ▽, $e/D = 0.1$; Sarpkaya (1977) ($Re = 10^5$); -----, $e/D = 0$, Sarpkaya & Rajabi (1979) ($Re = 10^5$).

3.4.2. *Influence of roughness*

Figures 26–28 compare the force coefficients obtained for the smooth and rough cylinders of the present study for the gap ratios $e/D = 1$ and 0.05. Figure 26 indicates that C_d increases substantially when the cylinder surface changes from smooth to rough. This is consistent with Sarpkaya's (1976b) wall-free cylinder data, corresponding to $Re = 10^5$. Figure 27 indicates that C_M does not significantly change with the change of surface roughness for $e/D = 1$. However, for $e/D = 0.05$, the inertial coefficient increases markedly when the surface of the cylinder changes from smooth to rough. This may be attributed to the retarding effect of the boundary layer at the wall side of the cylinder which may become significant for the inertia coefficient for small gap ratios such as 0.05.

Figure 28 shows that no significant change occurs in the lift coefficients when the surface is changed from smooth to rough. This result appears to be consistent with

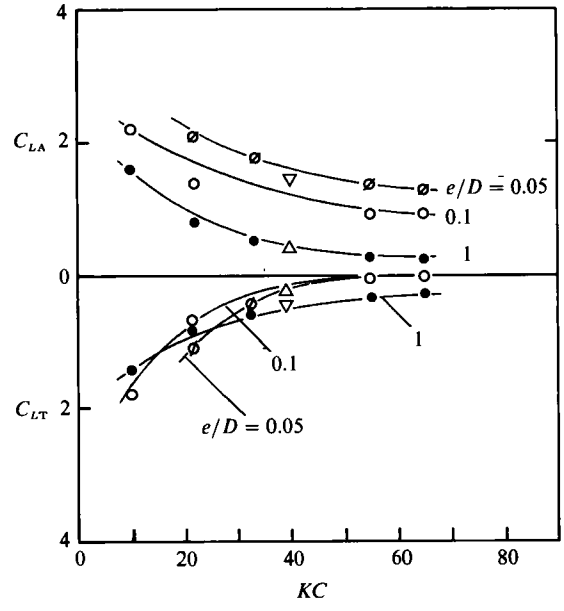

FIGURE 25. Lift-force coefficients. Symbols are the same as in figure 24.

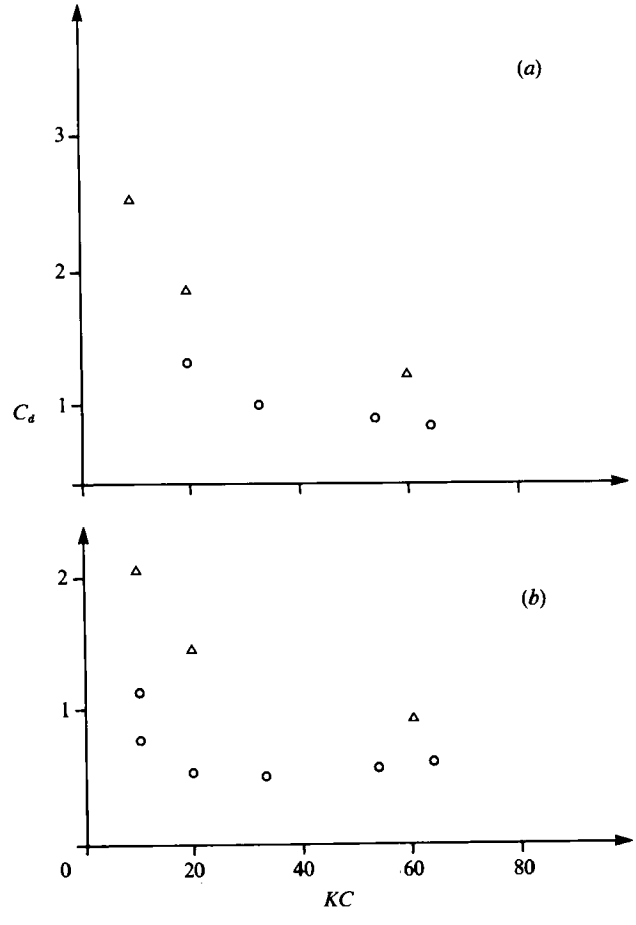

FIGURE 26. Drag coefficients for smooth (○) (Test series 1) and rough (△) (Test series 2) cylinders. $Re = 0.8 \times 10^5$–1.1×10^5. k/D of the rough cylinder $= 4 \times 10^{-3}$. (*a*) $e/D = 0.05$, (*b*) $e/D = 1$.

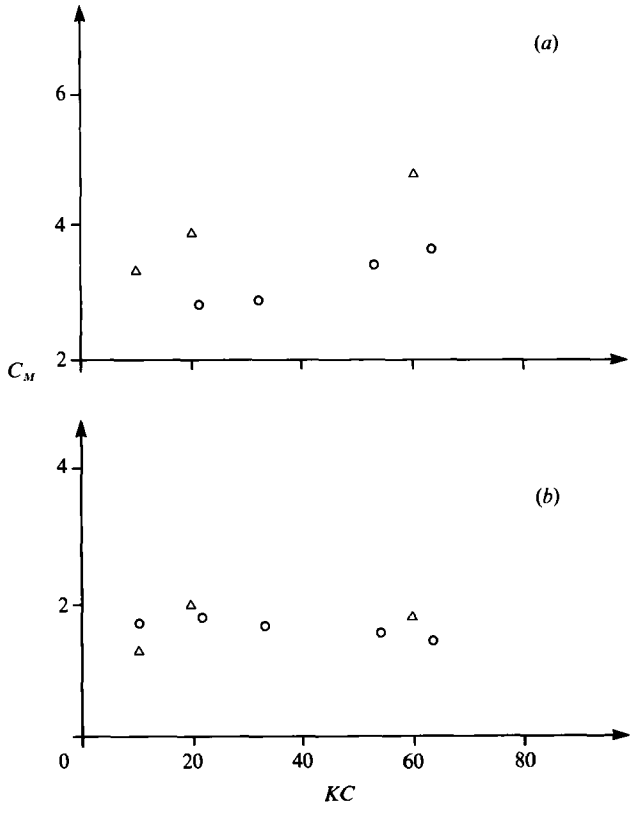

FIGURE 27. Inertia coefficients for smooth and rough cylinders. Symbols and conditions same as figure 26. (*a*) $e/D = 0.05$, (*b*) $e/D = 1$.

Sarpkaya's (1976*b*) wall-free cylinder results and also with Sarpkaya & Rajabi's (1979) wall-mounted cylinder results.

4. Summary and conclusions

Pressure measurements around a near-wall cylinder have been performed, and the results have been interpreted with the help of flow-visualization studies. The main results are summarized as follows.

(*a*) Symmetry in both the formation and motion of the vortices observed for a wall-free cylinder for $KC < 4$–5 disappears with the close proximity of a wall. An obvious consequence of this is the creation of a periodic lift force on the cylinder.

(*b*) The vortex flow regimes identified for wall-free cylinders (Williamson 1985) undergo tremendous changes with the close proximity of the wall when the gap-to-diameter ratios are below $O(1)$.

(*c*) The transverse vortex sheet observed for a wall-free cylinder for $7 < KC < 13$ disappears for values of the gap-to-diameter ratio below about 1.7.

(*d*) The vortex shedding is suppressed for small values of the gap ratio. The results indicate that the gap ratio below which the shedding is suppressed increases with increasing KC. For small KC, such as 10–20, the shedding persists for values of the gap ratio down to about $e/D = 0.1$. The shedding frequency itself is a function of e/D: it increases as e/D decreases.

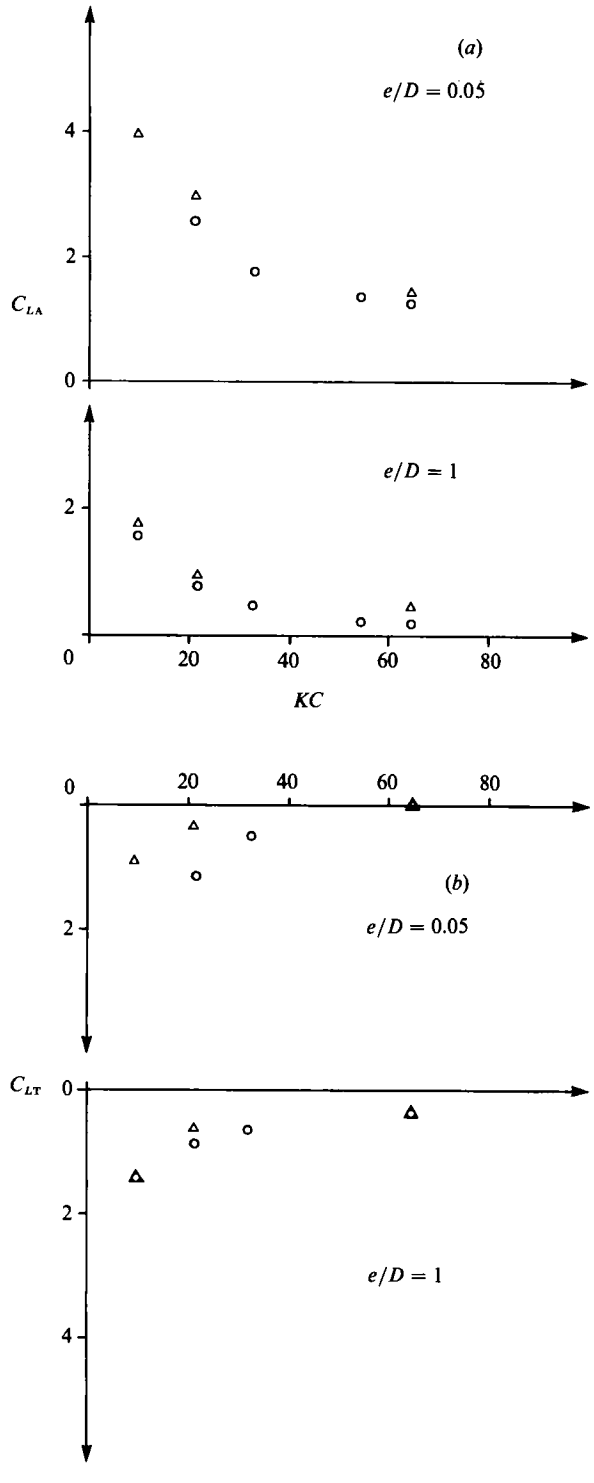

FIGURE 28. Lift-force coefficients for smooth and rough cylinders. Symbols and conditions same as figure 26. (*a*) Lift force away from the wall, (*b*) towards the wall.

(*e*) When the cylinder is placed very near the wall, the lift force experiences distinct, short-duration peaks, directed away from the wall. These peaks are associated with vortex shedding from the wall side of the cylinder.

(*f*) When the cylinder is placed on the wall, the main characteristic of the flow picture is the formation of a vortex pair each half-period prior to the creation of the lee-wake vortex behind the cylinder. This vortex pair steadily moves away from the cylinder, as the flow half-period progresses. The strong, single peak in the variation of the lift force is associated with the lee-wake vortex being washed over the cylinder.

This study is supported partially by the FTU project 'Turbulence around Offshore Structures' and the 'Marine Technique' programme of the Danish Scientific Council (STVF).

REFERENCES

ALI, N. & NARAYANAN, R. 1986 Forces on cylinders oscillating near a plane boundary. In *Proc. 5th Intl Offshore Mechanics & Arctic Engineering (OMAE) Symp., Tokyo, Japan*, vol. III, pp. 613–619.

BAGNOLD, R. A. 1974 Fluid forces on a body in shear-flow; experimental use of "stationary" flow. *Proc. R. Soc. Lond.* A **340**, 147–171.

BEARMAN, P. W. 1985 Vortex trajectories in oscillatory flow. In *Proc. Intl Symp. on Separated Flow Around Marine Structures, June 26–28*, p. 133. The Norwegian Inst. of Technology, Trondheim, Norway.

BEARMAN, P. W. & GRAHAM, J. M. R. 1979 Hydrodynamic forces on cylindrical bodies in oscillatory flow. In *Proc. 2nd Intl Conf. on the Behaviour of Offshore Structures, London*.

BEARMAN, P. W., GRAHAM, J. M. R., NAYLOR, P. & OBASAJU, E. D. 1981 The role of vortices in oscillatory flow about bluff cylinders. In *Proc. Intl Symp. on Hydrodyn. in Ocean Engr, Trondheim, Norway*.

BEARMAN, P. W., GRAHAM, J. M. R. & SINGH, S. 1979 Forces on cylinders in harmonically oscillating flow. In *Mechanics of Wave Induced Forces on Cylinders* (ed. T. L. Shaw). Pitman.

BEARMAN, P. W. & ZDRAVKOVICH, M. M. 1978 Flow around a circular cylinder near a plane boundary. *J. Fluid Mech.* **89**, 33–48.

BROWN, R. J. 1967 Hydrodynamic forces on a submarine pipeline. *J. Pipeline Div. ASCE* **93**, 9–19.

FREDSØE, J. & HANSEN, E. A. 1987 Lift forces on pipelines in steady flow. *J. Waterway, Port, Coastal Ocean Engng Div. ASCE* **113**, 139–155.

GÖKTUN, S. 1975 The drag and lift characteristic of a cylinder placed near a plane surface. M.Sc. thesis, Naval Post graduate School, Monterey, California.

GRASS, A. J. & KEMP, P. H. 1979 Flow visualization studies of oscillatory flow past smooth and rough circular cylinders. In *Mechanics of Wave-Induced Forces on Cylinders* (ed. T. L. Shaw). Pitman.

GRASS, A. J., RAVEN, P. W. J., STUART, R. J. & BRAY, J. A. 1984 The influence of boundary layer velocity gradients and bed proximity on vortex shedding from free spanning pipelines. *Trans. ASME J. Energy Resour. Tech.* **106**, 70–78.

JACOBSEN, V., BRYNDUM, M. B. & FREDSØE, J. 1984 Determination of flow kinematics close to marine pipelines and their use in stability calculations. In *Proc. 16th Annual Offshore Technology Conf. Paper* OTC 4833.

JENSEN, B. L., SUMER, B. M. & FREDSØE, J. 1989 Turbulent oscillatory boundary layers at high Reynolds numbers. *J. Fluid Mech.* **206**, 265–297.

JUSTESEN, P., HANSEN, E. A., FREDSØE, J., BRYNDUM, M. B. & JACOBSEN, V. 1987 Forces on and flow around near-bed pipelines in waves and current. In *Proc. 6th Intl Offshore Mechanics and Arctic Engineering Symp. Houston, Texas, March 1–6*, vol. II, pp. 131–138. ASME.

LUNDGREN, H., MATHIESEN, B. & GRAVESEN, H. 1976 Wave loads on pipelines on the seafloor. In *Proc. 1st Intl Conf. on the Behaviour of Off-Shore Structures* (BOSS 76), vol. I, pp. 236–247.

MAULL, D. J. & MILLINER, M. G. 1978 Sinusoidal flow past a circular cylinder. *Coastal Engng* **2**, 149–168.

MILNE-THOMPSON, L. M. 1962 *Theoretical Hydrodynamics*. Macmillan.

RAVEN, P. W. C., STUART, R. J. & LITTLEJOHNS, P. S. 1985 Full-scale dynamic testing of submarine pipeline spans. *17th Annual OTC in Houston, Texas, May 6–9, Paper* 5005.

ROSHKO, A., STEINOLFSON, A. & CHATTOORGOON, V. 1975 Flow forces on a cylinder near a wall or near another cylinder. In *Proc. 2nd US Conf. Wind Engrg Res., Fort Collins, Paper* IV-15.

SARPKAYA, T. 1976*a* Forces on cylinders near a plane boundary in a sinusoidally oscillating fluid. *Trans. ASME J. Fluids Engng* **98**, 499–505.

SARPKAYA, T. 1976 *b* In-line and transverse forces on smooth and sand-roughened cylinders in oscillatory flow at high Reynolds numbers. *Naval Postgraduate School, Monterey, California, Tech. Rep.* NPS-69SL76062.

SARPKAYA, T. 1977 In-line and transverse forces on cylinders near a wall in oscillatory flow at high Reynolds numbers. In *Proc. 9th Annual Offshore Technology Conf., Paper* OTC 2898.

SARPKAYA, T. 1987 Oscillating flow over bluff bodies in a U-shaped water tunnel. *AGARD Conf. Proc.*, 413, *Aerodynamic and Related Hydrodynamic Studies Using Water Facilities*, pp. 6–1.

SARPKAYA, T. & ISAACSON, M. 1981 *Mechanics of Wave Forces on Offshore Structures*. Van Nostrand Reinhold Company.

SARPKAYA, T. & RAJABI, F. 1979 Hydrodynamic drag on bottom-mounted smooth and rough cylinders in periodic flow. In *Proc. 11th Annual Offshore Technology Conf., Paper* OTC 3761.

SINGH, S. 1979 Forces on bodies in oscillatory flow. Ph.D. thesis, University of London.

SUMER, B. M. & FREDSØE, J. 1990 Scour below pipelines in waves. *J. Waterway, Port, Coastal Ocean Engng Div. ASCE* **116**, 307–323.

TANEDA, S. 1964 Experimental investigation of the wall effect on a cylindrical obstacle moving in a viscous fluid at low Reynolds numbers. *J. Phys. Soc. Japan* **19**, 1024–1030.

TANEDA, S. 1965 Experimental investigation of vortex streets. *J. Phys. Soc. Japan* **20**, 1714–1721.

WILLIAMSON C. H. K. 1985 Sinusoidal flow relative to circular cylinders. *J. Fluid Mech.* **155**, 141–174.

WRIGHT, J. C. & YAMAMOTO, T. 1979 Wave forces on cylinders near plane boundaries. *J. Waterway, Port, Coastal Ocean Engng Div. ASCE* **105**, 1–14.

YAMAMOTO, T., NATH, J. H. & SLOTTA, L. S. 1974 Wave forces on cylinders near plane boundary. *J. Waterway, Port, Coastal Ocean Engng Div. ASCE* **100**, 345–360.